Contrasting chemical environments in summertime for atmospheric ozone across major Chinese industrial regions: the effectiveness of emission control strategies

Zhenze Liu[1], Ruth M. Doherty[1], Oliver Wild[2], Michael Hollaway[2,a], and Fiona M. O'Connor[3]

[1]School of GeoSciences, The University of Edinburgh, UK
[2]Lancaster Environment Centre, Lancaster University, UK
[3]Met Office Hadley Centre, UK
[a]now at: Centre for Ecology & Hydrology, Lancaster Environment Centre, UK

Correspondence: Zhenze Liu (zhenze.liu@ed.ac.uk)

Abstract. The UKCA chemistry-climate model is used to quantify the differences in chemical environment for surface O_3 for six major industrial regions across China in summer 2016. We first enhance the UKCA gas-phase chemistry scheme by incorporating reactive VOC tracers that are necessary to represent urban and regional-scale O_3 photochemistry. We demonstrate that the model with the improved chemistry scheme captures the observed magnitudes and diurnal patterns of surface O_3 concentrations across these regions well. Simulated O_3 concentrations are highest in Beijing and Shijiazhuang on the North China Plain and in Chongqing, lower in Shanghai and Nanjing in the Yangtze River Delta, and lowest in Guangzhou in the Pearl River Delta despite the highest daytime O_3 production rates in Guangzhou. NO_x/VOC and H_2O_2/HNO_3 ratios indicate that O_3 production across all regions except Chongqing is VOC limited. We confirm this by constructing O_3 response surfaces for each region changing NO_x and VOC emissions and further contrast the effectiveness of measures to reduce surface O_3 concentrations. In VOC limited regions, reducing NO_x emissions by 20 % leads to a substantial O_3 increase (11 %) in Shanghai. We find that reductions in NO_x emissions alone of more than 70 % are required to decrease O_3 concentrations across all regions. Reductions in VOC emissions alone of 20 % produce the largest decrease (- 11 %) in O_3 levels in Shanghai and Guangzhou and the smallest decrease (- 1 %) in Chongqing. These responses are substantially different from those currently found in highly populated regions in other parts of the world, likely due to higher NO_x emission levels in these Chinese regions. Our work provides an assessment of the effectiveness of emission control strategies to mitigate surface O_3 pollution in these major industrial regions, and emphasizes that combined NO_x and VOC emission controls play a pivotal role in effectively offsetting high O_3 levels. It also demonstrates new capabilities in capturing regional air pollution that will permit this model to be used for future studies of regional air quality-climate interactions.

1 Introduction

Surface ozone (O_3) has become the main cause of atmospheric pollution in the summertime in China since 2013 and is particularly severe in industrial areas of China such as the North China Plain (NCP), the Yangtze River Delta (YRD), the Pearl River Delta (PRD) and the Sichuan basin where precursor emissions are high (Li et al., 2019a). The 90th percentile of the

maximum daily 8-hour average (MDA8) O_3 concentration in 30 of 74 major cities of China exceeded the National Ambient Air Quality Standard (100 ppb) in summer, 2017 (Wang et al., 2017; Lu et al., 2018; Silver et al., 2018; Li et al., 2019b; Lu et al.,

25   2019a). During 2013-2017, the national Air Pollution Prevention and Control Action Plan has successfully reduced emissions of fine particulate matter ($PM_{2.5}$) and nitrogen oxides ($NO_x = NO + NO_2$) in China by 33 % and 21 %, respectively (Zheng et al., 2018). However, the reduction in NO_x emissions has led to an increase in O_3 levels in polluted areas due to the non-linear chemistry of O_3 and reduced titration of O_3 by NO (Li et al., 2019a; Wang et al., 2019). Volatile organic compounds (VOCs) are also important O_3 precursors and emissions of these have increased across China over the same period, exacerbating O_3

30   pollution (Zheng et al., 2018). VOC emissions are believed to have decreased in megacity regions such as Beijing (Cheng et al., 2019), but the resulting O_3 decrease is likely to have been offset by the O_3 increase due to reduced NO_x emissions. This poses a challenge to mitigate surface O_3 pollution. Therefore, the balance of emission controls on NO_x and VOC is critical to decreasing O_3 levels in these regions.

    O_3 is a secondary photochemical pollutant in the troposphere that can be produced rapidly through oxidation of its precursors

35   NO_x, VOCs and carbon monoxide (CO) in the presence of sunlight. Power plants, industry, residences, and transport are the main anthropogenic sources of NO_x and VOC emissions (Monks et al., 2015; Li et al., 2018a). Isoprene is the principal biogenic VOC and is released from trees, plants and crops (Sindelarova et al., 2014). O_3 formation is mainly initiated through oxidation of VOC species by hydroxyl radicals (OH). The resulting organic peroxy radicals (RO_2) and hydroperoxyl radicals (HO_2) can convert NO to NO_2 without destroying O_3. O_3 is then created from the combination of $O(^3P)$ atoms, formed from photolysis

40   of the resulting NO_2, and oxygen (O_2) (Sillman, 1999; von Schneidemesser et al., 2015; Wang et al., 2017). Under low NO_x conditions, HO_2 radicals may combine to produce hydrogen peroxide (H_2O_2). However, at high NO_x concentrations, nitric acid (HNO_3) and organic nitrates (RO_2NO_2) are easily formed as NO_2 reacts with OH and RO_2. HNO_3 and RO_2NO_2 are the main sinks of radicals and are readily removed from the atmosphere by deposition. Therefore, increasing NO_x concentrations increase O_3 production, but also accelerate the formation of HNO_3 and RO_2NO_2, leading to less efficient O_3 formation. In

45   addition, direct titration of O_3 by NO becomes increasingly important at higher levels of NO_x. There is hence a transition in the magnitude of O_3 production from low to high NO_x conditions. This turnover is dependent on the local chemical environment, and in particular on the relative abundance of NO_x and VOCs (Sillman, 1995; Kleinman et al., 1997; Thornton et al., 2002; Kleinman et al., 2005; Sillman and West, 2009).

    A variety of O_3 sensitivity indicators have been proposed to characterise the O_3 response to changing precursor emissions.

50   The simplest of these are based on the concentration ratios of the precursors, NO_x/VOCs, or of their oxidation products, H_2O_2/HNO_3 (Sillman, 1995). O_3 concentrations increase with NO_x emissions and are not sensitive to VOC emissions in a NO_x limited regime when NO_x concentrations are relatively low (Sillman et al., 1990). However, in a VOC limited regime, O_3 levels may increase with decreasing NO_x emissions, which is common in urban areas with high NO_x emissions, and this is reflected in high NO_x/VOC or low H_2O_2/HNO_3 ratios. Critical values of these indicators of O_3 sensitivity vary by region

55   and by season (Sillman, 1995; Liu et al., 2010; Xing et al., 2019). Most major industrial regions in China are believed to be VOC limited and rural areas are NO_x limited or in a transition regime (Jin and Holloway, 2015; Wang et al., 2017). O_3 production efficiency (OPE) is another important metric to evaluate the impacts of NO_x emissions on O_3 concentrations (Liu

et al., 1987; Kleinman et al., 2002). This is defined as the number of O_3 molecules produced per molecule of NO_x oxidised. Low OPE values are typically associated with high NO_x conditions and indicate that there is less O_3 produced from a given

60 amount of NO_x. OPE values generally increase as NO_x emissions decrease, reflecting greater O_3 production per molecule of NO_x oxidised at lower NO_x levels.

In this study, we develop new capabilities in a global scale model by incorporating higher VOC chemistry, allowing the model to represent the oxidation environment in major industrialised regions in China. We focus on the spatial and temporal variation of daytime O_3 in this study. We first evaluate the performance of this global chemistry-climate model in simulating

65 regional O_3 across large industrialised regions. We use O_3 sensitivity indicators to compare and contrast the chemical oxidative environment across these different regions in China to identify emission control measures that would be most beneficial to reduce O_3 pollution levels. Using a global model novelly allows us to compare the impact of emission control measures in China with those in other major industrialised regions across the world. The value of this approach is that the same model set-up can be used to assess the impact of future emission and climate scenarios, studies of tropospheric and stratospheric O_3

70 influences and comparisons of O_3 in different parts of world.

The configuration of the model used in this study is described in section 2, along with its development and application to surface O_3 in China. We evaluate the model performance in reproducing the diurnal cycles of surface O_3 and NO_2 in section 3, and we investigate the O_3 chemical environment in China, including O_3 precursor concentrations and sensitivity ratios in section 4. We calculate the local O_3 production rates, O_3 loss rates, NO_x loss rates and OPE in section 5. We then quantify the

75 O_3 responses to changing NO_x and VOC emissions in these regions and investigate the requirements of emission controls to reduce O_3 levels in each region in sections 6 and 7. To provide a global context we compare and contrast the effectiveness of emission control strategies with that in other parts of the world in section 7 and present our conclusions in section 8.

2 Materials and methods

2.1 Model description, development and application

80 The United Kingdom Chemistry and Aerosols (UKCA) model is a state-of-the-art chemistry and aerosol model that simulates atmospheric composition from the troposphere to the upper stratosphere. It is coupled to the Met Office Hadley Centre's Global Environment Model (HadGEM) family of climate models, all of which are based on the UK Unified Model (MetUM) (O'Connor et al., 2014). It is also the atmospheric composition component of the UK Earth System Model (UKESM) (Sellar et al., 2019). Version 10.6.1 of UKCA is used in this study, coupled with the Global Atmosphere 7.1 (GA7.1) configuration

85 (Walters et al., 2019) of HadGEM3 (Hewitt et al., 2011). The spatial resolution is N96L85 with 1.875° by longitude and 1.25° by latitude, and there are 85 terrain-following hybrid height layers with a model top at 85 km. The model time step is 20 minutes for meteorology, and chemistry is calculated every hour. Wind speed and temperature are nudged with ERA-interim reanalyses from the European Centre for Medium-Range Weather Forecasts (ECMWF) every 6 hours (Dee et al., 2011). Sea surface temperature and sea ice fields are prescribed with the climatology mean of 1995-2004 (Reynolds et al., 2007).

90   The Stratosphere-Troposphere (Strat-Trop) gas-phase chemical scheme is used to simulate the inorganic odd oxygen (O_x), hydrogen ($HO_x = OH + HO_2$) and NO_x chemical cycles, oxidation of CO and VOCs, chlorine and bromine chemistry, and heterogeneous processes on aerosols (Archibald et al., 2020). The Global Model of Aerosol Processes (GLOMAP) aerosol scheme is used with a two-moment pseudo-modal aerosol dynamics approach to simulate sulfate, sea-salt, dust, black carbon and both primary and secondary organic aerosol (Mann et al., 2010). Interactive photolysis is represented with Fast-JX which

95   derives photolysis rates between 177 and 750 nm (Neu et al., 2007).

Global chemistry-climate models typically include simplified gas-phase chemistry schemes representing a limited number of species to mitigate high computational demands. Major long-lived VOC species are selected and more reactive VOC species are typically omitted from the chemistry scheme (Young et al., 2018). Eight discrete emitted VOC species (formaldehyde (HCHO), ethane (C_2H_6), propane (C_3H_8), acetaldehyde (CH_3CHO), acetone (($CH_3)_2CO$), methanol (CH_3OH), isoprene

100   (C_5H_8) and monoterpene ($C_{10}H_{16}$) are simulated in the Strat-Trop chemistry scheme of UKCA. This selection is appropriate for simulating the global burden of O_3 but is less suitable for simulating O_3 concentrations in high emission areas. In industrial regions of China, large abundances of more reactive VOCs such as alkenes and aromatics make substantial contributions to O_3 production (Wu and Xie, 2017; Tan et al., 2019; Liu et al., 2020). To address this, we incorporate more reactive classes of VOC including alkenes, higher alkanes and aromatics, represented by propene (C_3H_6), butane (C_4H_{10}) and toluene (C_7H_8)

105   respectively in the chemistry scheme (Atkinson et al., 2006; Folberth et al., 2006). This permits a more realistic simulation of photochemically active environments, and allows rapid O_3 formation in high VOC emission regions to be captured. The improved chemistry scheme includes 101 species, 244 bimolecular reactions, 26 uni- and termolecular reactions, 70 photolytic reactions, 5 heterogeneous reactions and 3 aqueous phase reactions for the sulfur cycle.

We perform model simulations for 2016 and focus our results on summer (June-July-August, JJA). We spin up the model

110   for 4 months and then simulate the full year nudged with ERA-interim reanalysis data for 2016. The new capabilities of the model allow us to investigate regional O_3 chemical environment in industrial regions of China in the model. The relatively coarse resolution of the model may lead to biases in surface O_3 associated with numerical diffusion (Wild and Prather, 2006; Stock et al., 2014; Fenech et al., 2018; Mertens et al., 2020), but we note that the lifetime of O_3 makes it a regional-scale pollutant except very close to high emission sources (Valari and Menut, 2008; Hodnebrog et al., 2011; Biggart et al., 2020).

115   This study demonstrates the first application of this improved chemistry scheme to high emission regions worldwide, and lays the foundation for more detailed studies of the interactions between air quality and climate in a global chemistry-climate model under future scenarios.

2.2 Emissions

The anthropogenic emission inventory of Hemispheric Transport of Air Pollution (HTAP) for 2010 is used for the globe

120   outside China (Janssens-Maenhout et al., 2015). The Multi-resolution Emission Inventory for China (MEIC) is used to provide emissions over China for 2013 (Li et al., 2017). We apply independent diurnal and vertical profiles to each emission sector (industry, power plants, transport and residences) according to European Monitoring and Evaluation Programme (EMEP) emissions (Bieser et al., 2011; Mailler et al., 2013). Biogenic VOC (BVOC) emissions are calculated interactively through

the Joint UK Land Environmental Simulator (JULES) land-surface scheme in UKCA (Pacifico et al., 2011). The Global Fire Emissions Database (GFED4) are used for biomass burning emissions (van der Werf et al., 2010). Other aspects of the emissions used are as described in Archibald et al. (2020).

Given the rapid changes in anthropogenic emissions across China, we adjust NO_x, VOCs, CO, sulphur dioxide (SO_2), black carbon (BC) and organic carbon (OC) emissions in MEIC from 2013 to 2016 by applying national and urban emission scaling factors. NO_x emissions decreased by 18.8 % and VOC emissions increased slightly by 1.1 % between 2013 and 2016 across China (Zheng et al., 2018). NO_x and VOC emissions are estimated to have decreased by 24.2 % and 12.8 % respectively in Beijing and surrounding areas between 2013 and 2016 (Cheng et al., 2019). We apply the Beijing scaling factors to major industrialised regions, reflecting tighter emission controls in these developed urban regions, and use national scaling factors across the rest of the country.

2.3 Selected regions and observations

We focus on six heavily populated regions with high emissions within the major industrialised regions in China. These include Beijing and Shijiazhuang on the North China Plain (32 – 40 °N, 114 – 121°E), Shanghai and Nanjing in the Yangtze River Delta (28 – 33 °N, 118 – 123 °E), Guangzhou in the Pearl River Delta (21 – 25 °N, 111 – 115 °E) and Chongqing in the Sichuan Basin (28 – 32 °N, 103 – 108 °E), see Fig. 1. Anthropogenic NO_x and VOC emissions are high in these regions (Fig. 2) due to rapid industrialisation, urbanization and socio-economic development. Model grid cells that include observation stations located in each of the urban and rural regions are selected to be representative of these regions, see Table 1. For comparison with observations, we calculate a grid-weighted mean according to the number of measurement sites in each model grid cell for the region.

We use observed hourly concentrations of air pollutants including O_3 and NO_2 from the surface monitoring networks of China, obtained from the public website https://quotsoft.net/air/ which mirrors data from the Chinese National Environmental Monitoring Centre (CNEMC) http://www.cnemc.cn/. There are 1,670 national measurement stations that started operating in 2013.
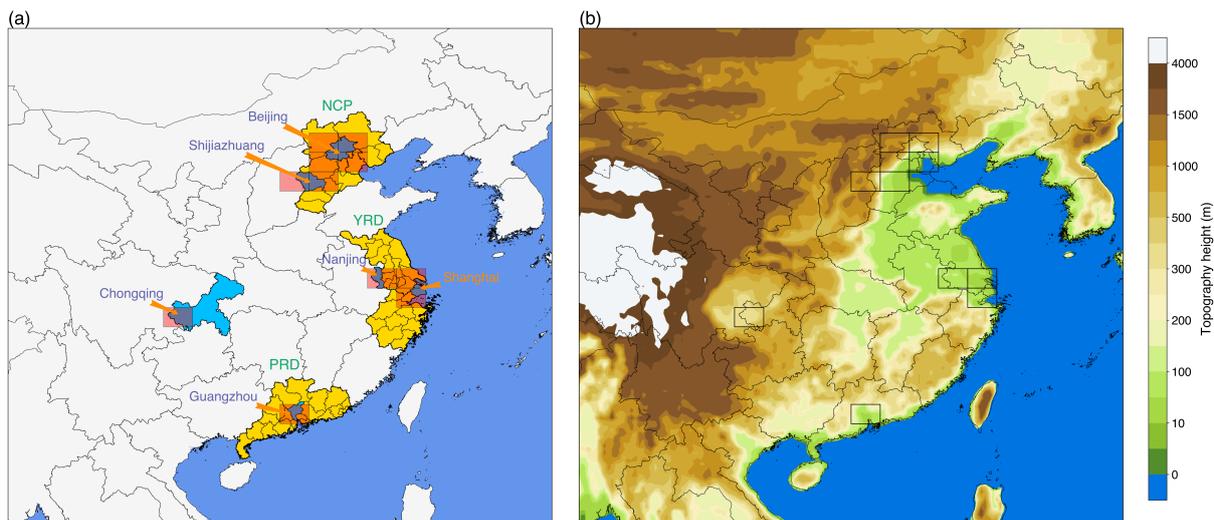
Figure 1. Map of China showing **(a)** the key provinces (yellow) representing the NCP, the YRD and the PRD and locations of the six regions (blue) – Beijing, Shijiazhuang, Shanghai, Nanjing, Guangzhou and Chongqing, and UKCA model grid cells co-located with these regions (red) **(b)** elevations across the whole of China.
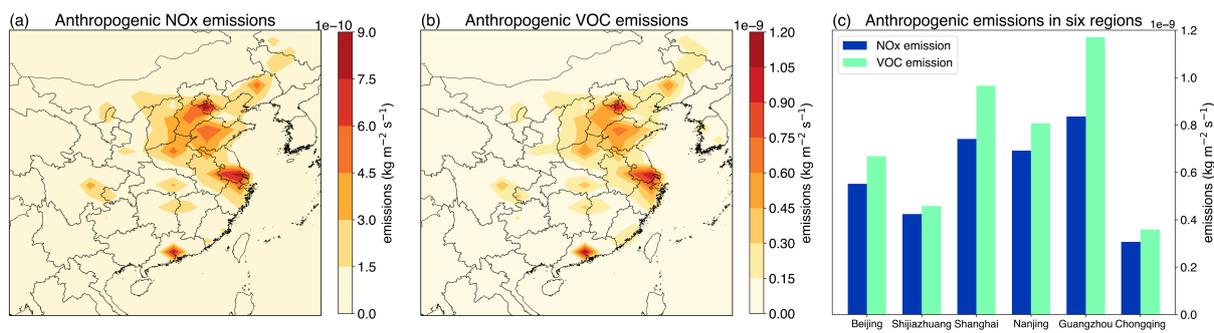
Figure 2. Spatial distributions of anthropogenic NO_x and VOC emissions ($kg\,m^{-2}\,s^{-1}$) across China **(a, b)** and grid-weighted averaged emissions for the six regions within the four major industrialised regions **(c)** in JJA, 2016.

Table 1. Number of measurement sites and grid cells in the six industrial regions

Region	No. of measurement sites	No. of grid cells
Beijing	46	4
Shijiazhuang	28	2
Shanghai	58	2
Nanjing	45	1
Guangzhou	45	1
Chongqing	25	1

3 Model evaluation of surface O_3 and NO_2

We evaluate the diurnal variation in simulated surface O_3 and NO_2 concentrations against summertime observations for JJA, 2016 for the six industrialised regions (Fig. 3, 4). In general, the diurnal variation of observed O_3 is matched relatively well and the correlation coefficients are relatively high, see Table 2. Mean concentrations for O_3 and NO_2 over the lowest three model layers (from the surface up to 130 m) are also compared with observations. In the daytime, differences between the surface and three lowest layers are small due to efficient mixing in the planetary boundary layer (PBL). The height of the nocturnal PBL is typically underestimated in the model leading to overestimated NO_x concentrations and hence underestimated O_3 concentrations at nighttime due to excessive O_3 titration by NO (André et al., 1978; Petersen et al., 2019; Zhao et al., 2019). Fig. 3a shows a large difference in nighttime O_3 concentrations across the three layers, reflecting stable conditions that allow NO_x to accumulate at the surface. Simulated surface O_3 concentrations therefore tend to be underestimated at nighttime. In contrast, the peaks in daytime O_3 concentrations are captured relatively well, reflecting efficient O_3 production in the high VOC environment.

Daily mean O_3 concentrations for Beijing, Shijiazhuang, Shanghai and Guangzhou are reproduced well with small biases (~10 %; see Table 2). Simulated daily mean O_3 concentrations are highest (> 40 ppb) for Beijing, Shijiazhuang and Chongqing, lower in Shanghai and Nanjing (< 40 ppb), and lowest for Guangzhou (~30 ppb). Although daily mean O_3 concentrations are captured relatively well, as seen in Fig. 3a and 4a, daytime maximum O_3 concentrations are overestimated, associated with underestimated NO_2 concentrations. This overestimation is largest in Shijiazhuang where the underestimation of daytime NO_2 concentrations is larger than other regions. We find that there is a systematic bias in Chongqing where simulated O_3 levels are higher than observations. Chongqing is a mountainous inland region with complex topography that cannot be fully resolved, and surface O_3 here is thus representative of higher surface altitudes leading to a systematic bias high compared with observations (Su et al., 2018), and a corresponding bias low for NO_2 concentrations. In addition, simulated O_3 increases from biogenic emissions in the Sichuan basin are much larger in summertime than other regions (Lu et al., 2019b), and uncertainty in these emissions may contribute to the biases.

The diurnal patterns in NO_2 concentrations can also be captured as reflected by high levels at nighttime and low levels in the daytime for all regions. Daytime NO_2 concentrations can be reproduced relatively well, with a small underestimation. While

this may reflect underestimated NO_x emissions, it is more likely to arise from the effects of dilution on NO_x. High emissions in these regions are diluted over a large grid cell, resulting in lower NO_2 concentrations in the daytime. This is offset by high NO_2 concentrations in the PBL at nighttime as discussed above. The diurnal variation of NO_2 concentrations is hence stronger in the simulations than the observations (Fig. 4a).

Fig. 3 and 4 also show the frequency distribution of observed and modelled hourly O_3 and NO_2 concentrations. The simulated peaks in the distributions of O_3 and NO_2 are underestimated compared to observations for all six regions, reflecting the larger diurnal variation in the simulations. The diurnal variation is more closely simulated for O_3 concentrations (correlation coefficient r > 0.7) than for NO_2 concentrations. The Chongqing region has the closest correlation with observations (r = 0.83), which provides evidence that the overestimation of O_3 is systematic as suggested earlier. Overall, the magnitudes (see Table 2) and diurnal patterns (see Fig. 3 and 4) of both species can be simulated reasonably well, with differences between industrial regions clearly captured.

Table 2. Comparison of modelled and observed daily mean surface O_3 and NO_2 concentrations for the six industrial regions in JJA, 2016, China.

Region	Obs. (ppb)	Sim. (ppb)	Bias ppb/%	RMSE (ppb)	Correlation r
O_3					
Beijing	47.7±22.1	43.4±27.7	-4.4 (9.1%)	8.1	0.77
Shijiazhuang	42.9±18.4	47.6±28.7	4.7 (10.9%)	11.6	0.78
Shanghai	38.3±17.5	34.4±28.8	-3.9 (10.2%)	12.7	0.77
Nanjing	42.6±18.9	35.9±24.9	-6.8 (15.8%)	9.8	0.71
Guangzhou	29.8±18.3	28.0±25.9	-1.8 (-6.1%)	9.4	0.81
Chongqing	38.1±19.2	56.0±31.3	18.0 (47.2%)	22.3	0.83
NO_2					
Beijing	17.8±3.7	20.7±8.2	2.9 (16.2%)	5.8	0.69
Shijiazhuang	18.1±4.7	16.7±8.3	-1.4 (7.7%)	4.3	0.76
Shanghai	16.3±2.3	26.1±8.7	9.8 (60.0%)	12.1	0.50
Nanjing	17.2±3.6	21.3±9.0	4.1 (23.7%)	7.8	0.49
Guangzhou	16.1±3.0	19.9±9.3	3.8 (23.7%)	8.4	0.55
Chongqing	17.4±3.8	10.9±6.3	-6.4 (37.1%)	8.0	0.43
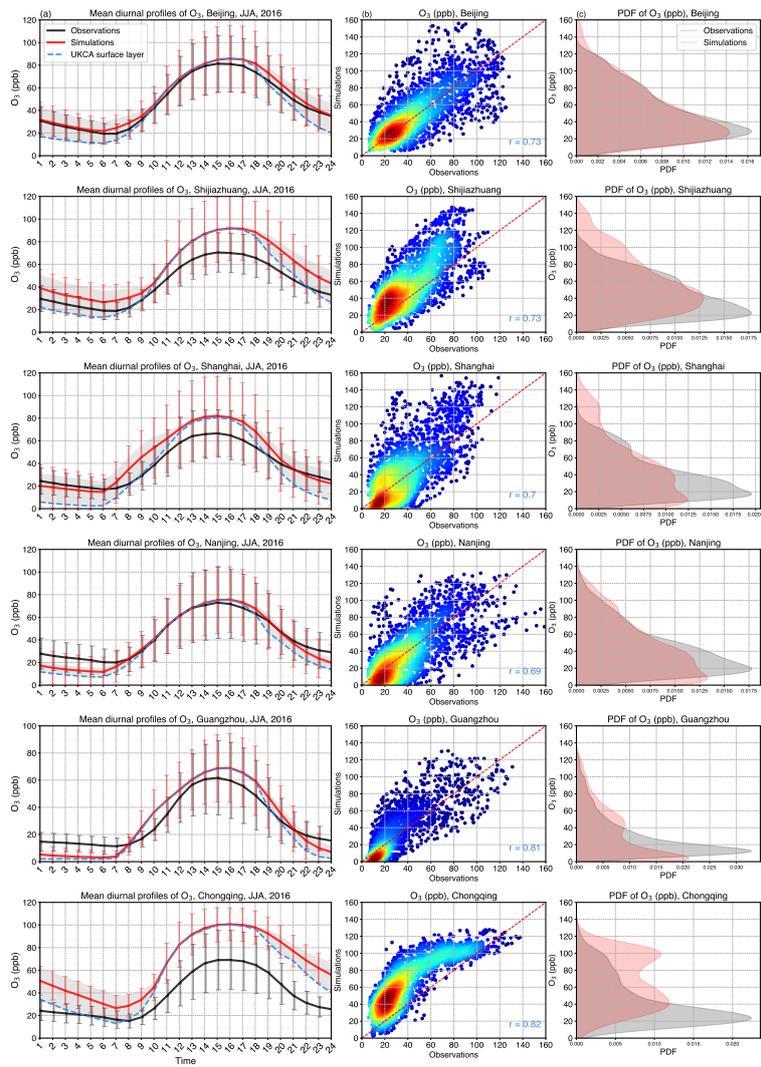
Figure 3. Comparison of observed and modelled O_3 concentrations for the six industrialised regions in JJA, 2016, China. **(a)** Mean diurnal cycles of observed and modelled O_3 concentrations (ppb). The shaded area represents the spread across the lowest three model layers. Error bars denote one standard deviation of hourly O_3 concentrations across all days **(b)** Observed and modelled hourly O_3 concentrations (ppb; three lowest model layers) and correlation coefficient values r **(c)** PDF of O_3 concentrations (ppb) for modelled and observed hourly values.
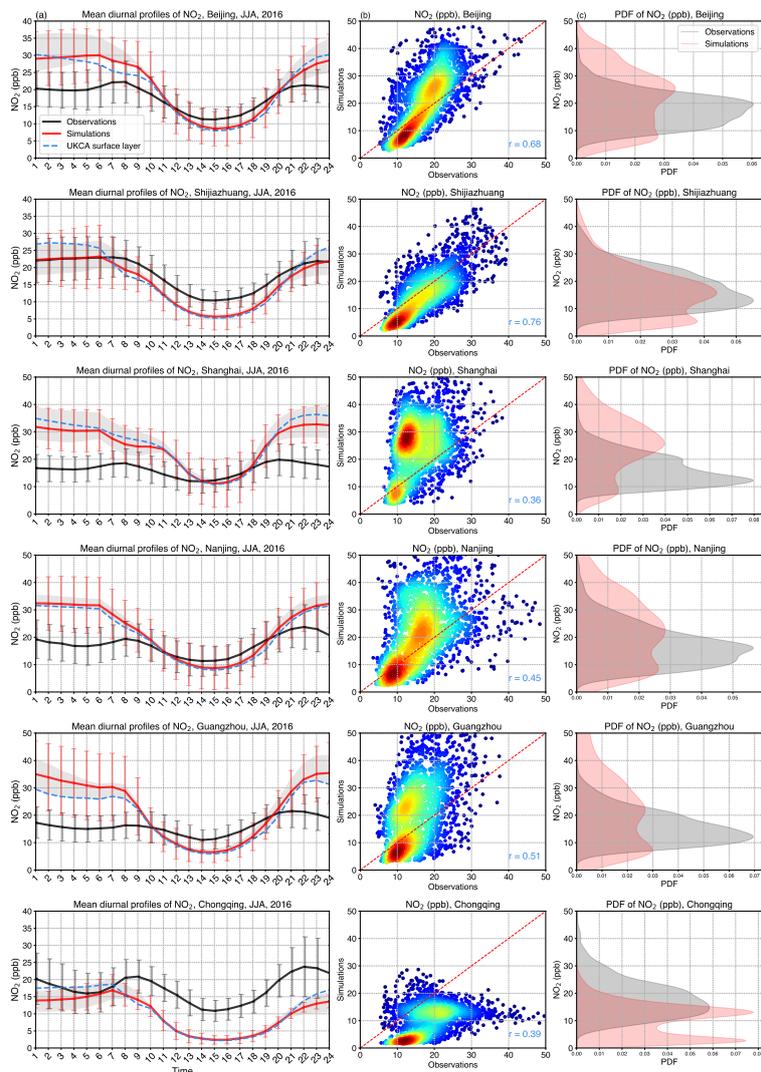
Figure 4. Comparison of observed and modelled NO_2 concentrations for the six industrialised regions in JJA, 2016, China. **(a)** Mean diurnal cycles of observed and modelled NO_2 concentrations (ppb). The shaded area represents the spread across the lowest three model layers. Error bars denote one standard deviation of hourly NO_2 concentrations across all days. **(b)** Observed and modelled hourly NO_2 concentrations (ppb; three lowest model layers) and correlation coefficient values r **(c)** PDF of NO_2 concentrations (ppb) for modelled and observed hourly values.

4 Differences in chemical environment

Spatial distributions of modelled daytime concentrations of O_3, NO_x, VOCs and O_3 sensitivity ratios (NO_x/VOCs and H_2O_2/HNO_3) are shown in Fig. 5 to illustrate the differences in chemical environment for the six regions. We focus on daytime hours with the highest O_3 concentrations using the MDA8 metric and consider this same time period for other species, which we refer to

hereafter as daytime concentrations. For the sensitivity ratio NO$_x$/VOCs we consider the sum of anthropogenic and biogenic daytime VOC concentrations.
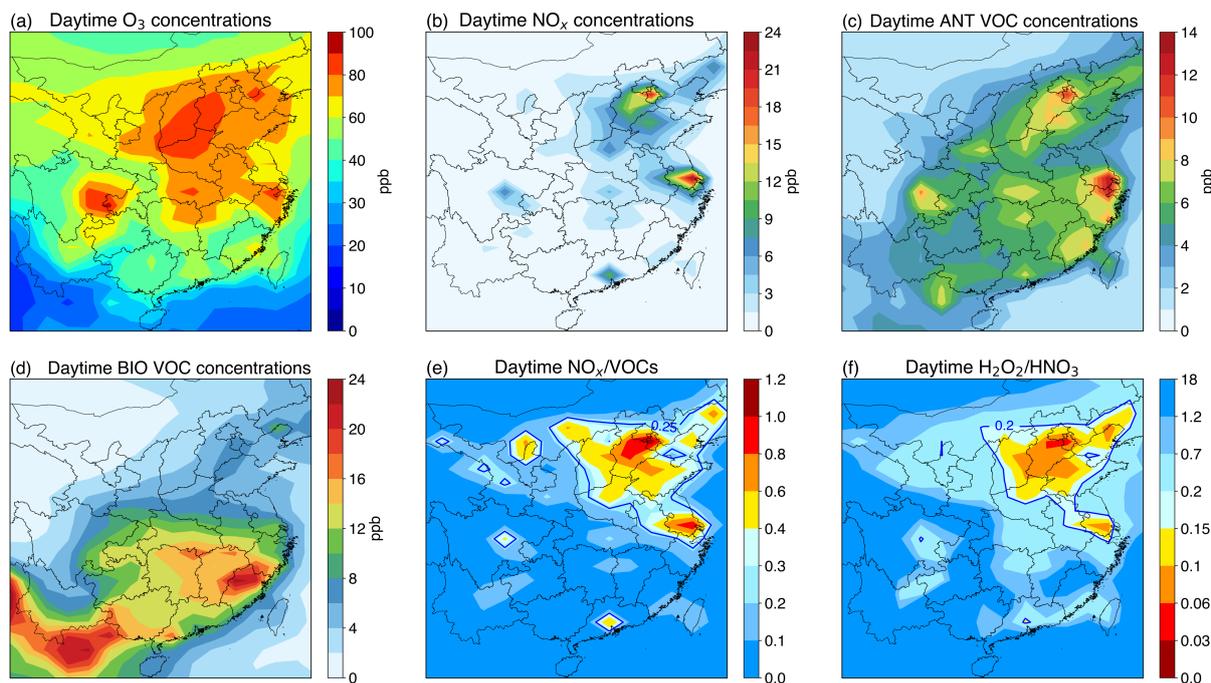
Figure 5. Spatial distributions of simulated surface daytime O$_3$, NO$_x$, anthropogenic VOCs, biogenic VOCs (ppb) **(a, b, c, d)** and two O$_3$ sensitivity ratios – NO$_x$/VOCs and H$_2$O$_2$/HNO$_3$ **(e, f)** in JJA, 2016, China.

Figure 5a shows high daytime O$_3$ levels (> 80 ppb) across northern China, eastern China and the Sichuan basin in JJA, 2016.

190 O$_3$ levels in the PRD (~40 ppb) are much lower despite high emissions likely due to transport of clean air from the South China Sea associated with the East Asian summer monsoon (Zhao et al., 2010; Li et al., 2018b). Areas with high anthropogenic NO$_x$ and VOC concentrations generally coincide with high emission regions (Fig. 2, Fig. 5b, 5c). High daytime NO$_x$ concentrations (> 12 ppb) are simulated in Beijing and Shijiazhuang, Shanghai and Nanjing. Chongqing has the lowest NO$_x$ concentrations of 3–6 ppb due to relatively low NO$_x$ emissions. High anthropogenic daytime VOCs concentrations are simulated across the

195 main industrial regions, in particular in Shanghai with the highest levels (> 12 ppb; Fig 5c).

The distribution of biogenic VOC concentrations differs from that of anthropogenic VOCs (Fig. 5c, 5d). There is a strong latitudinal gradient, reflecting differences in climate and the spatial distribution of vegetation (Li et al., 2013). The highest biogenic VOC levels (> 16 ppb) are simulated in south-eastern China where deciduous and mixed broadleaf trees are the main source of biogenic VOCs. The YRD, the PRD and the Sichuan basin have higher biogenic VOC concentrations than the NCP.

200 Chongqing has the highest biogenic VOC levels (> 12 ppb) of the regions considered here. However, highest biogenic VOC levels are found south of China in Laos, Vietnam and Cambodia.

High NO_x/VOC ratios and low H_2O_2/HNO_3 ratios typically indicate VOC limited O_3 production. The transition between VOC and NO_x limited regimes is typically about 0.25 for the NO_x/VOC ratio and about 0.2 for the H_2O_2/HNO_3 ratio (Liu et al., 2010; Xing et al., 2019). From these two thresholds for the O_3 sensitivity ratios, it can be seen that VOC limited regions cover most areas of the NCP, parts of the YRD including Shanghai and Nanjing, and Guangzhou in the PRD (Fig. 5e, 5f). All six regions except Chongqing have NO_x/VOCs ratios $\geq$ 0.6 and H_2O_2/HNO_3 ratios $\leq$ 0.18 (Table 3). This suggests that these regions have a chemical environment that is strongly VOC limited. In addition, VOC limited regimes shown by both indicators are quite similar, showing that these two O_3 sensitivity ratios may be useful to directly diagnose different O_3 sensitivity regimes in China. Regions with high NO_x/VOC ratios and low H_2O_2/HNO_3 ratios typically occur where NO_x concentrations are high. Overall, these transition values delineate the different O_3 sensitivity regions across China well, showing VOC limited regimes in the major industrial regions with high emissions. However, we note that these O_3 sensitivity ratios only provide an estimate of the chemical environment, and further, more detailed investigation of O_3 responses to emission changes are required.

Table 3. Simulated surface daytime concentrations of species, radicals, O_3 sensitivity ratios and the photolysis rate $j(O^1D)$ for the six industrial regions in JJA, 2016, China.

Region	Beijing	Shijiazhuang	Shanghai	Nanjing	Guangzhou	Chongqing
Species (ppb)						
O_3	78.0	83.5	70.1	66.8	60.2	93.8
NO_x	12.8	8.7	19.2	12.9	10.7	3.8
VOC (ANT)	8.7	7.0	12.7	7.6	7.5	7.7
VOC (BIO)	5.5	4.3	10.6	9.2	10.2	13.5
VOC (Total)	14.3	11.3	23.3	16.9	17.7	21.3
Sensitivity ratios						
NO_x/VOCs	0.79	0.73	0.89	0.78	0.60	0.18
H_2O_2/HNO_3	0.18	0.08	0.10	0.11	0.09	0.29
Radicals						
OH / 10^6 cm^{-3}	7.8	10.3	8.4	9.8	13.0	16.6
HO_2 / 10^8 cm^{-3}	2.6	2.9	2.3	2.2	2.2	7.4
RO_2 / 10^8 cm^{-3}	1.0	0.9	0.8	0.8	0.9	2.5
Photolysis rate						
$j(O^1D)$/ 10^{-5} s^{-1}	2.3	2.6	2.3	2.5	3.1	3.4

5   Differences in local O_3 production rates

In this section, we calculate the daytime production rates for surface O_3 to investigate how the local O_3 production compares across the six regions. We define the net O_3 production rate (ppb/h) as the gross rate of production $P(O_3)$ from the reactions

HO$_2$ + NO and RO$_2$ + NO minus the gross rate of loss L(O$_3$) from the reactions O(^{1}D) + H$_2$O, O$_3$ + OH, O$_3$ + HO$_2$ and O$_3$ + VOCs. We assume that the pathways above represent the net O$_3$ production rate under O$_3$ photochemical steady state between NO and NO$_2$, and are shown as follows:

$$Net\ P(O_3) = P(O_3) - L(O_3) =$$
$$k_1[HO_2][NO] + k_2[RO_2][NO] - (k_3[O(^1D)][H_2O] + k_4[O_3][OH] + k_5[O_3][HO_2] + k_6[O_3][VOCs]) \quad (1)$$

where k_i represents the rate coefficient of reaction i.

The loss of NO$_x$, L(NO$_x$), is principally determined by the reactions OH + NO$_2$ and RO$_2$ + NO$_2$ which produce HNO$_3$ and RO$_2$NO$_2$, respectively. OPE is then defined as the number of O$_3$ molecules produced per molecule of NO$_x$ consumed (Liu et al., 1987).

$$OPE = \frac{P(O_3)}{L(NO_x)} \quad (2)$$

As shown in Fig. 6, local O$_3$ production varies across the six regions with O$_3$ net production rates ranging from 4-10 ppb/h. Simulated daytime net O$_3$ production rates are highest (> 8 ppb/h) in Shanghai and Guangzhou mainly due to high precursor emissions, and this is reflected by higher O$_3$ concentrations in Shanghai than in nearby Nanjing. While O$_3$ production is high in Guangzhou, the O$_3$ concentrations are much lower than in other regions, indicating that meteorological impacts in this coastal region are important to transport O$_3$ produced locally. O$_3$ net production in Beijing and Shijiazhuang is similar to that in Nanjing (~5 ppb/h). O$_3$ production in Chongqing is also high, reflecting high radical concentrations (see Table 3) that promote O$_3$ production despite lower precursor emissions. High photolysis rates j(O(^{1}D)) in Chongqing and Guangzhou contribute to high concentrations of OH radicals (Table 3). O$_3$ destruction rates are fairly similar (< 4 ppb/h) across these regions, but are higher in Chongqing, offsetting its high O$_3$ production rates.
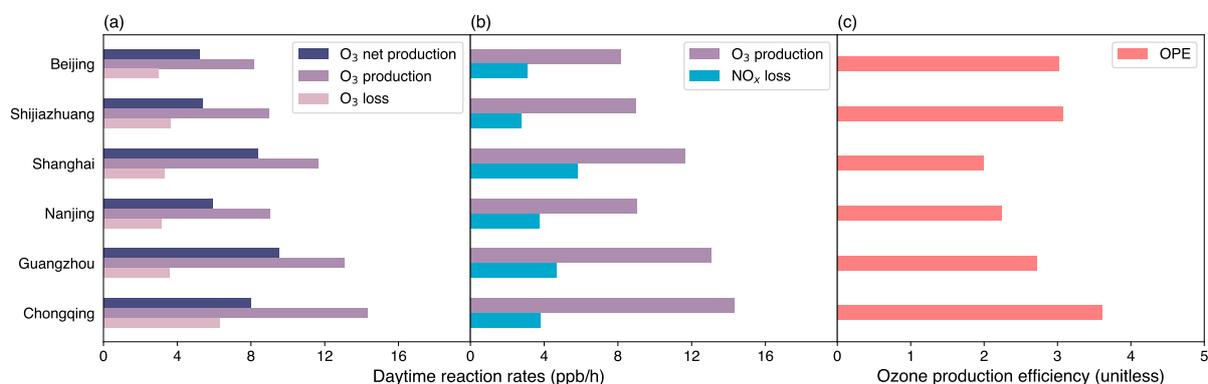
Figure 6. Simulated surface daytime **(a)** net O$_3$ production rates, gross O$_3$ production rates and gross O$_3$ loss rates (ppb/h) **(b)** gross O$_3$ production rates and NO$_x$ loss rates (ppb/h) **(c)** OPE (unitless) for the six industrial regions in JJA, 2016, China.

235   The simulated NO_x loss rates (Fig. 6b) show the highest removal of NO_x in Shanghai, where NO_x concentrations are also highest. This influences OPE, which is strongly dependent on NO_x loss, and leads to the lowest OPE in Shanghai and highest in Chongqing (Fig. 6c). The low OPE in Shanghai and Nanjing shows the low efficiency in O_3 production per molecule of NO_x consumed. However, the OPE values in all six regions are generally lower than those in other remote and rural regions, in agreement with Wang et al. (2018), indicating that high precursor emissions in these regions are the main cause of high surface

240   O_3 concentrations.

6   Response of O_3 to emission controls

We quantify the response of daytime O_3 to emission changes to investigate the relationship between the chemical environment and the magnitude of O_3 changes for the six industrial regions of China. We implement three scenarios applying 20 % reductions in anthropogenic NO_x emissions, VOC emissions and combined NO_x and VOC emissions.

245   Spatial distributions of simulated daytime surface O_3 responses vary across China (Fig. 7). In the 20 % NO_x emission control scenario, substantial O_3 increases (2-10 ppb) can be seen in the NCP, the YRD and the PRD, and O_3 concentrations decrease (0-8 ppb) in the Sichuan basin. In the 20 % VOC emission control scenario, there are small O_3 changes in most non-industrial regions of China (-1–2 ppb) but O_3 concentrations generally decrease by 1-9 ppb across the NCP, the YRD and the PRD. The Sichuan basin shows relatively small O_3 decreases. Areas showing O_3 increases in the 20 % NO_x emission control experiment

250   match well with VOC limited areas indicated by the NO_x/VOCs and H_2O_2/HNO_3 ratios (cf. Fig. 5e, 5f vs Fig. 7a) suggesting that all the industrial regions considered here are VOC limited except Chongqing in the Sichuan basin that is NO_x limited.
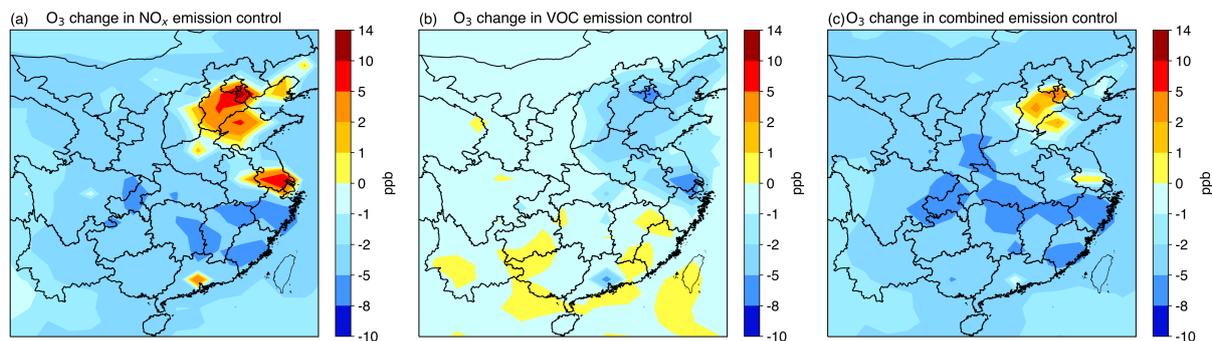
Figure 7. Spatial distributions of simulated surface daytime O_3 concentration changes (ppb) for **(a)** the 20 % NO_x emission control, **(b)** the 20 % VOC emission control and **(c)** the 20 % combined NO_x and VOC emission control compared to the present-day results in JJA, 2016, China.

In general, the greatest O_3 increases in the 20 % NO_x control scenario occur in areas with high precursor concentrations. Shanghai shows the largest O_3 increases (11 %) (Table 4) and has the highest underlying NO_x concentrations (Table 3). O_3 increases in Beijing and Guangzhou are similar (~8 %) possibly because of their similar NO_x concentrations. Shijiazhuang

255   in the NCP shows the smallest O_3 increase (4 %) because of its lower NO_x concentrations. In contrast, an O_3 decrease of

4 % is seen in Chongqing that is NO_x limited. In the 20 % VOC control scenario, the largest O_3 decreases are simulated in Shanghai and Guangzhou (-10 %) while minimal O_3 decreases (-1 %) are simulated in Chongqing. The chemical environment in Chongqing is NO_x limited and therefore the O_3 changes are not sensitive to VOC emissions.

Table 4. Simulated daytime mean O_3 concentrations and changes in NO_x, VOC and combined NO_x and VOC emission controls for the six industrial regions in JJA, 2016, China.

O_3 (ppb)/ Region	Base	NO_x control	Change (%)	VOC control	Change (%)	NO_x+VOC control	Change (%)
Beijing	78.0	84.7	8.6%	72.5	-7.0%	79.7	2.2%
Shijiazhuang	83.5	86.6	3.8%	80.2	-3.9%	84.6	1.4%
Shanghai	70.1	77.8	11.0%	63.1	-10.0%	69.4	-1.0%
Nanjing	66.8	72.4	8.5%	61.4	-8.0%	67.8	1.6%
Guangzhou	60.2	64.8	7.6%	53.8	-10.7%	60.4	0.3%
Chongqing	93.8	89.5	-4.6%	92.5	-1.4%	88.5	-5.6%

In addition to separate 20 % reductions in NO_x and VOC emissions, we demonstrate the importance of combined NO_x and VOC emission controls to mitigate O_3 pollution in VOC limited regions. This effectively offsets the higher levels of O_3 that arise with NO_x emission reductions alone. The O_3 increase in Shanghai is fully offset in the combined emission control (-1 %). While O_3 increases still occur in the other VOC limited regions, these increases are minimal (< 3 %). Reducing both NO_x and VOC emissions decreases O_3 levels in Chongqing by 6 %. Therefore, combined emission controls are necessary to efficiently mitigate O_3 pollution in all these industrial regions, and VOC emission controls should be at least as stringent as NO_x emission controls to address rising O_3 levels in these industrial regions.

7 Effectiveness of emission controls in reducing surface O_3 levels

To provide a more complete exploration of the effectiveness of emission controls, we construct a response surface of summertime daytime O_3 for each region to show the effect of changing NO_x and VOC emissions. We do this by performing a set of 64 model simulations with global anthropogenic NO_x and VOC emissions scaled independently over the range 0-140 % in increments of 20 %.

Figure 8 shows the magnitude and direction of O_3 changes in the six regions as NO_x and VOC emissions change. For context, Fig. 8a also shows the simulated daytime O_3 changes between 2013 and 2019 in the Beijing region following estimated emission changes (Cheng et al., 2019). We find that simulated O_3 concentrations in Beijing increase from 71.6 ppb in 2013 to 82.6 ppb in 2019, an increase of 1.8 ppb/year. This is consistent with observed changes of 1.9 ppb/year over this period due to anthropogenic emission changes (Li et al., 2020). The observed daytime O_3 concentrations are 83 ppb in the Beijing region in 2019. This demonstrates that the model captures not only the magnitude and diurnal pattern of O_3 in summer 2016 well but also the observed O_3 changes in recent years.
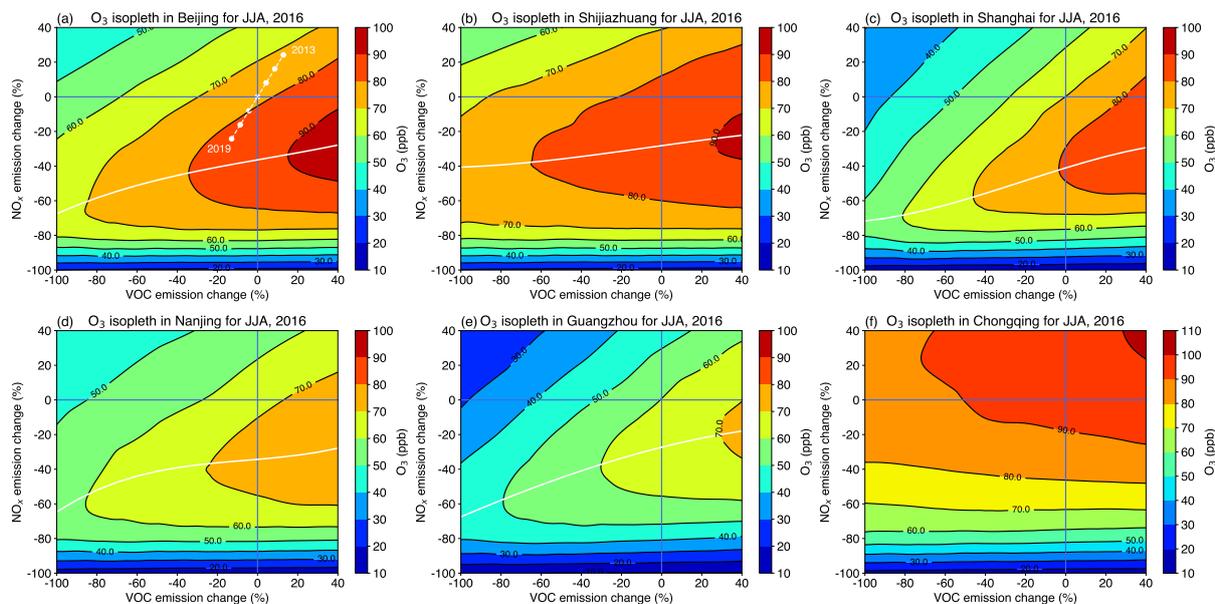
Figure 8. Simulated daytime surface O_3 responses (ppb) to anthropogenic NO_x and VOC emission changes for the six industrial regions across China **(a – f)** in JJA, 2016. The intersection of the vertical and horizontal lines marks current O_3 levels. White ridge lines mark the peak in O_3 concentrations for given VOC emissions, and show the approximate transition between VOC limited (above the ridge) and NO_x limited (below the ridge) regimes. White dots in **(a)** represent simulated daytime O_3 levels in the Beijing region in JJA between 2013 and 2019 following estimated NO_x and VOC emission changes.

The patterns of O_3 response seen in the VOC limited regions (Fig. 8a-e) are similar, such that decreases in NO_x emissions from their current levels increase O_3 concentrations. Large O_3 increases occur in Shanghai and Beijing, highlighting that it is not beneficial to reduce NO_x emissions unless VOC emissions are also reduced. Large reductions (~40 %) in NO_x emissions are required to shift the chemical environment from VOC limited to NO_x limited for these two regions. The large decrease in O_3 in Shanghai and Guangzhou when reducing VOC emissions indicates that the efficiency in lowering O_3 levels by decreasing VOC emissions is high in these regions. In contrast, the efficiency of VOC emissions alone in reducing O_3 levels is lower in Shijiazhuang and Chongqing.

Figure 9 shows the O_3 responses in each region to changes in NO_x emissions, VOC emissions and combined NO_x and VOC emissions, which represent cross-sections through the O_3 response surfaces shown in Fig 8. It is difficult to decrease O_3 concentrations in Shanghai by reducing NO_x emissions alone because there is a steep rise in surface O_3 (~15 %) when NO_x emissions are reduced by 40 % from the current state. Decreasing O_3 from current levels requires reductions in NO_x emissions of more than 50 % for Shijiazhuang and Guangzhou and more than 70 % for Beijing, Shanghai and Nanjing. This suggests that mitigating poor O_3 air quality in these VOC limited regions through NO_x emission controls alone would require much greater reductions than the 21 % reductions in NO_x emissions that are reported to have occurred in China from 2013 to 2017 (Zheng et al., 2018).
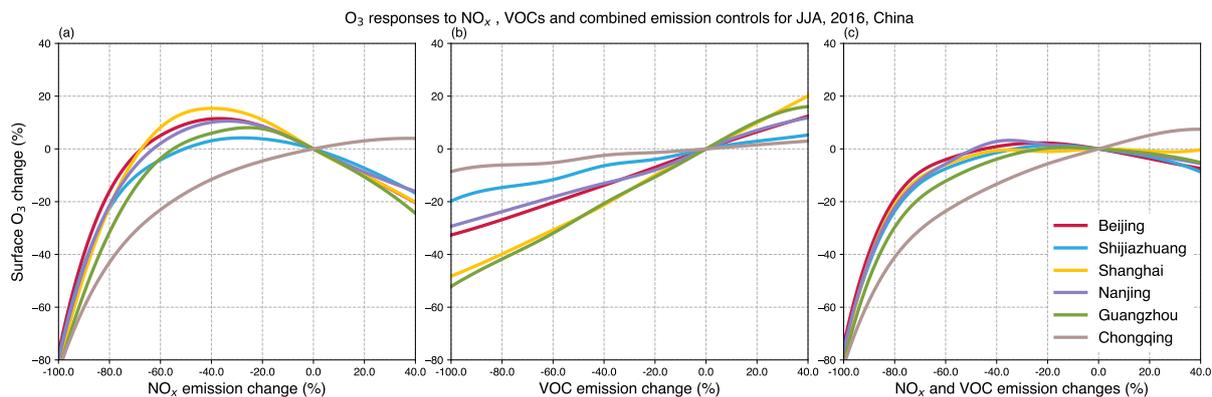
Figure 9. Simulated daytime surface O_3 responses to changes in anthropogenic emissions of **(a)** NO_x, **(b)** VOC and **(c)** combined NO_x and VOC emissions for the six industrial regions in JJA, 2016, China.

O_3 responses to VOC emission changes are smaller and more linear than the responses seen for NO_x emissions changes (Fig. 9a, 9b). Reducing VOC emissions by 40 % gives large decreases in O_3 concentrations (20 %) in Shanghai and Guangzhou and

295 smaller decreases (< 10 %) in Shijiazhuang and Chongqing (Fig. 9b). Reductions in VOC emissions are key to reducing present-day O_3 concentrations as they effectively offset the rising O_3 levels due to decreasing NO_x emissions (Fig. 9c). Emission reductions of 50 % or more are required to reduce O_3 levels for all regions if controls on NO_x and VOC emissions are applied simultaneously.

To place our results in a wider global context, Figure 10 shows summer-mean surface O_3 changes over different regions

300 with high emissions in other parts of the world compared with those in China. We consider six major industrialised regions outside of China and select the model grid-cell that is most closely co-located with the region. We note that proportional increases in summer-mean O_3 are larger than that of daytime O_3 increases when NO_x emissions are reduced (see Fig. 9), principally because absolute O_3 concentrations are smaller with the inclusion of nighttime conditions. We find that all selected high emission regions across the globe outside of China are NO_x limited, such that NO_x emissions decreases yield regional

305 O_3 decreases. Current levels of NO_x emissions in these regions are considerably lower than for the industrial regions of China, reflecting the different O_3 sensitivity regimes (Table 5).
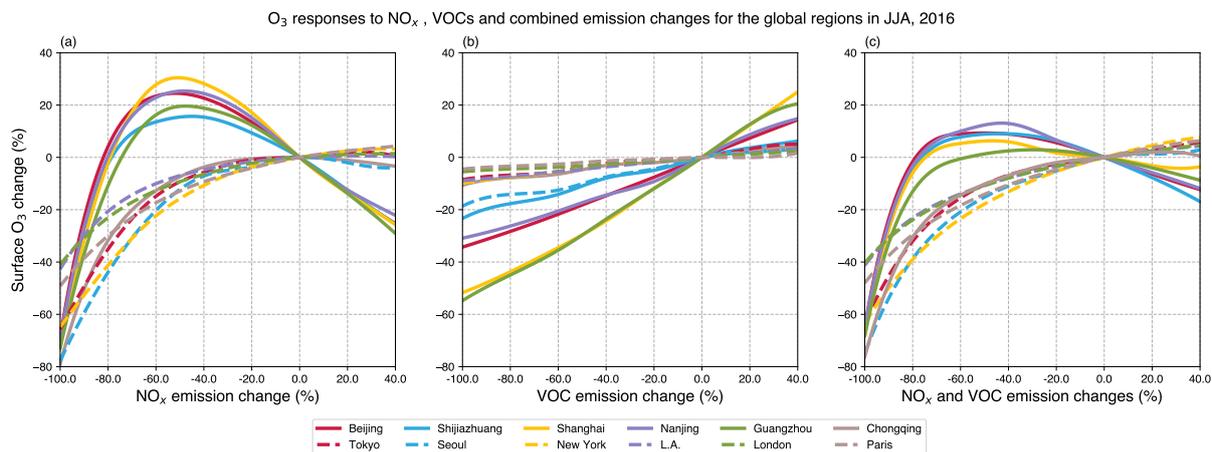
Figure 10. Simulated summertime mean surface O_3 responses to anthropogenic **(a)** NO_x, **(b)** VOC and **(c)** combined NO_x and VOC emission changes in regions across the globe: Tokyo, Seoul, New York, L.A., London, Paris (dashed lines) and those in major industrial regions of China (solid lines) in JJA, 2016.

Reductions of both NO_x and VOC emissions substantially decrease O_3 levels for these selected regions outside of China, and the magnitude of the O_3 decreases are similar to those found for Chongqing (Fig 10). Conversely, the magnitude of O_3 decreases when reducing VOC emissions are smaller than all five VOC limited regions in China. This indicates that O_3 concentrations are less sensitive to VOC emissions in these other world regions due to their lower VOC emissions (Table 5).

Despite lower NO_x and VOC emissions in the regions outside of China, surface O_3 concentrations, particularly in the Seoul and New York regions, are similar to those for China. This highlights that regional O_3 levels also depend on background O_3 concentrations, despite localised NO_x and VOC emissions that lead to different O_3 production regimes. The O_3 levels in European regions e.g. London and Paris are lowest, in accordance with the lowest NO_x and VOC emission levels. Overall, these results show that there are substantial differences in the efficiency of emission control scenarios to reduce surface O_3 levels in different parts of the world. For many industrial regions of China, the extended regions are VOC limited and hence, reductions of VOC emissions are the key to reducing poor O_3 air quality. For other regions selected in this study NO_x emission reductions are still pertinent to improving O_3 pollution.

Table 5. Anthropogenic NO_x and VOC emissions ($*e^{-10}$ kg m^{-2} s^{-1}) and summertime mean surface O_3 concentrations (ppb) in regions across the industrial regions of China and the globe. MEIC emissions of 2013 adjusted for 2016 are used for Chinese industrial regions. HTAP emissions of 2010 are used for other regions of the globe.

Region	NO_x emissions	VOC emissions	O_3 conc.
China			
Beijing	5.5	6.7	43.4
Shijiazhuang	4.2	4.6	47.6
Shanghai	7.4	9.6	34.4
Nanjing	6.9	8.1	35.9
Guangzhou	8.4	12.0	28.0
Chongqing	3.1	3.6	56.0
Global			
Tokyo	2.0	2.6	38.9
Seoul	1.5	2.1	45.5
New York	2.3	3.1	45.3
L.A.	1.1	1.3	40.1
London	1.1	1.5	30.6
Paris	0.8	1.0	32.6

8 Conclusions

320 This study presents the application of the global chemistry-climate UKCA model with an improved gas-phase chemistry scheme including more reactive VOCs to simulate regional summertime O_3 pollution across major industrialised regions in China for the first time. Differences in atmospheric chemical environments are investigated, and the effectiveness of different emission control strategies in reducing O_3 concentrations is quantified. The model captures the magnitude, diurnal profiles and diurnal variation of O_3 concentrations across most industrial regions well. We highlight that peak O_3 concentrations can be

325 captured well, indicating that O_3 production can be effectively simulated with more highly active VOC oxidation environments for high emission regions of China.

Simulated daytime O_3 levels are highest on the North China Plain (Beijing and Shijiazhuang), and in the Sichuan Basin (Chongqing), and are lowest in the Pearl River Delta (Guangzhou). We find that there is a systematic bias in O_3 throughout the diurnal cycle in Chongqing reflecting the mountainous inland area that is inadequately captured by the topography in the

330 model. The O_3 production rates are highest in the Pearl River Delta compared to other regions. However, its much lower O_3 levels reflect the importance of meteorological impacts in this coastal region. OPE values in these industrial regions are low, indicating that their high O_3 levels are mainly caused by high precursor emissions. Both O_3 sensitivity ratios we apply here (NO_x/VOCs and H_2O_2/HNO_3) suggest that all the industrial regions except Chongqing are VOC limited.

A set of simulations are performed with a range of NO_x and VOC emissions to construct O_3 response surfaces to assess the impacts of different emission control strategies in different regions. Reducing NO_x emissions alone by 20 % leads to a substantial O_3 increase (11 %) in Shanghai. Reductions in VOC emissions alone of 20 % produce the largest decrease (-11 %) in O_3 levels in Shanghai and Guangzhou and the smallest decrease (- 1 %) in Chongqing. We find that reducing O_3 concentrations across all industrial regions of China would require more than 70 % reductions if reducing NO_x emissions alone, and therefore VOC emission controls are important to reduce O_3 levels. We also find that combined emission controls effectively offset high O_3 levels that arise from reduced NO_x emissions alone. These responses are substantially different from those currently found in major highly populated regions in other parts of the world. The results show NO_x limited O_3 production in these global areas, which also reflects the predominance of heavily populated VOC limited areas across the industrial regions in China. Therefore, O_3 pollution in the industrial regions of China should be treated as a regional issue and regional VOC emission control strategies should be considered.

The new capabilities for simulating regional surface O_3 pollution developed here will be helpful for future model studies to investigate the regional O_3 impacts on climate. The magnitude of O_3 changes over recent years in the Beijing region can be reproduced well. There remain model biases in regions with complex topography and high elevation – a common issue for global and regional models. Another source of uncertainty is the rapid change in anthropogenic emissions in recent years in China, which presents a particular challenge for inventory development. Recently, while NO_x emissions have been successfully reduced across many regions in China, changes in VOC emissions have been relatively small, and this has led to an increase in O_3 concentrations in many regions. Regional VOC emission controls are hence urgently needed to maximise the effectiveness in reducing surface O_3 pollution in China.

Data availability. The data generated in this study will be made available through the Edinburgh DataShare at https://datashare.is.ed.ac.uk/handle/xxxxx.

Author contributions. ZL, RD and OW designed the study. ZL, MH and FO'C set up the model. ZL ran model simulations and performed the analysis. ZL, RD and OW prepared the paper with contributions from all co-authors.

Competing interests. The authors declare that they have no conflict of interest.

Acknowledgements. ZL thanks the University of Edinburgh China Scholarship Council. MH, OW and RD thank the Natural Environment Research Council (NERC) for funding under grants NE/N006925/1, NE/N006976/1 and NE/N006941/1. This work made use of computation resources on the Met Office and NERC joint supercomputer system (MONSooN) in the UK. ZL thanks the UKCA community for help in the model set-up.

References

André, J. C., Moor, G. D., Lacarrère, P., and Vachat, R. d.: Modeling the 24-Hour Evolution of the Mean and Turbulent Structures of the Planetary Boundary Layer, Journal of Atmospheric Sciences, 35, 1861-1883, 1978.

Archibald, A. T., O'Connor, F. M., Abraham, N. L., Archer-Nicholls, S., Chipperfield, M. P., Dalvi, M., Folberth, G. A., Dennison, F., Dhomse, S. S., Griffiths, P. T., Hardacre, C., Hewitt, A. J., Hill, R. S., Johnson, C. E., Keeble, J., Kohler, M. O., Morgenstern, O., Mulcahy, J. P., Ordonez, C., Pope, R. J., Rumbold, S. T., Russo, M. R., Savage, N. H., Sellar, A., Stringer, M., Turnock, S. T., Wild, O., and Zeng, G.: Description and evaluation of the UKCA stratosphere-troposphere chemistry scheme (StratTrop vn 1.0) implemented in UKESM1, Geoscientific Model Development, 13, 1223-1266, 10.5194/gmd-13-1223-2020, 2020.

Atkinson, R., Baulch, D. L., Cox, R. A., Crowley, J. N., Hampson, R. F., Hynes, R. G., Jenkin, M. E., Rossi, M. J., and Troe, J.: Evaluated kinetic and photochemical data for atmospheric chemistry: Volume II - gas phase reactions of organic species, Atmospheric Chemistry and Physics, 6, 3625-4055, 10.5194/acp-6-3625-2006, 2006.

Bieser, J., Aulinge, A., Matthias, V., Quante, M., and van der Gon, H.: Vertical emission profiles for Europe based on plume rise calculations, Environmental Pollution, 159, 2935-2946, 10.1016/j.envpol.2011.04.030, 2011.

Biggart, M., Stocker, J., Doherty, R. M., Wild, O., Hollaway, M., Carruthers, D., Li, J., Zhang, Q., Wu, R. L., Kotthaus, S., Grimmond, S., Squires, F. A., Lee, J., and Shi, Z. B.: Street-scale air quality modelling for Beijing during a winter 2016 measurement campaign, Atmospheric Chemistry and Physics, 20, 2755-2780, 10.5194/acp-20-2755-2020, 2020.

Cheng, J., Su, J. P., Cui, T., Li, X., Dong, X., Sun, F., Yang, Y. Y., Tong, D., Zheng, Y. X., Li, Y. S., Li, J. X., Zhang, Q., and He, K. B.: Dominant role of emission reduction in PM2.5 air quality improvement in Beijing during 2013-2017: a model-based decomposition analysis, Atmospheric Chemistry and Physics, 19, 6125-6146, 10.5194/acp-19-6125-2019, 2019.

Dee, D. P., Uppala, S. M., Simmons, A. J., Berrisford, P., Poli, P., Kobayashi, S., Andrae, U., Balmaseda, M. A., Balsamo, G., Bauer, P., Bechtold, P., Beljaars, A. C. M., van de Berg, L., Bidlot, J., Bormann, N., Delsol, C., Dragani, R., Fuentes, M., Geer, A. J., Haimberger, L., Healy, S. B., Hersbach, H., Holm, E. V., Isaksen, L., Kallberg, P., Kohler, M., Matricardi, M., McNally, A. P., Monge-Sanz, B. M., Morcrette, J. J., Park, B. K., Peubey, C., de Rosnay, P., Tavolato, C., Thepaut, J. N., and Vitart, F.: The ERA-Interim reanalysis: configuration and performance of the data assimilation system, Quarterly Journal of the Royal Meteorological Society, 137, 553-597, 10.1002/qj.828, 2011.

Fenech, S., Doherty, R. M., Heaviside, C., Vardoulakis, S., Macintyre, H. L., and O'Connor, F. M.: The influence of model spatial resolution on simulated ozone and fine particulate matter for Europe: implications for health impact assessments, Atmospheric Chemistry and Physics, 18, 5765-5784, 10.5194/acp-18-5765-2018, 2018.

Folberth, G. A., Hauglustaine, D. A., Lathiere, J., and Brocheton, F.: Interactive chemistry in the Laboratoire de Meteorologie Dynamique general circulation model: model description and impact analysis of biogenic hydrocarbons on tropospheric chemistry, Atmospheric Chemistry and Physics, 6, 2273-2319, 10.5194/acp-6-2273-2006, 2006.

Hewitt, H. T., Copsey, D., Culverwell, I. D., Harris, C. M., Hill, R. S. R., Keen, A. B., McLaren, A. J., and Hunke, E. C.: Design and implementation of the infrastructure of HadGEM3: the next-generation Met Office climate modelling system, Geoscientific Model Development, 4, 223-253, 10.5194/gmd-4-223-2011, 2011.

Hodnebrog, O., Stordal, F., and Berntsen, T. K.: Does the resolution of megacity emissions impact large scale ozone?, Atmospheric Environment, 45, 6852-6862, 10.1016/j.atmosenv.2011.01.012, 2011.

Janssens-Maenhout, G., Crippa, M., Guizzardi, D., Dentener, F., Muntean, M., Pouliot, G., Keating, T., Zhang, Q., Kurokawa, J., Wankmuller, R., van der Gon, H. D., Kuenen, J. J. P., Klimont, Z., Frost, G., Darras, S., Koffi, B., and Li, M.: HTAP_v2.2: a mosaic of regional and global emission grid maps for 2008 and 2010 to study hemispheric transport of air pollution, Atmospheric Chemistry and Physics, 15, 11411-11432, 10.5194/acp-15-11411-2015, 2015.

Jin, X. M., and Holloway, T.: Spatial and temporal variability of ozone sensitivity over China observed from the Ozone Monitoring Instrument, Journal of Geophysical Research-Atmospheres, 120, 7229-7246, 10.1002/2015jd023250, 2015.

Kleinman, L. I., Daum, P. H., Lee, J. H., Lee, Y. N., Nunnermacker, L. J., Springston, S. R., Newman, L., WeinsteinLloyd, J., and Sillman, S.: Dependence of ozone production on NO and hydrocarbons in the troposphere, Geophysical Research Letters, 24, 2299-2302, 10.1029/97gl02279, 1997.

Kleinman, L. I., Daum, P. H., Lee, Y. N., Nunnermacker, L. J., Springston, S. R., Weinstein-Lloyd, J., and Rudolph, J.: Ozone production efficiency in an urban area, Journal of Geophysical Research-Atmospheres, 107, 10.1029/2002jd002529, 2002.

Kleinman, L. I., Daum, P. H., Lee, Y. N., Nunnermacker, L. J., Springston, S. R., Weinstein-Lloyd, J., and Rudolph, J.: A comparative study of ozone production in five U.S. metropolitan areas, Journal of Geophysical Research-Atmospheres, 110, 10.1029/2004jd005096, 2005.

Li, K., Jacob, D. J., Liao, H., Shen, L., Zhang, Q., and Bates, K. H.: Anthropogenic drivers of 2013-2017 trends in summer surface ozone in China, Proceedings of the National Academy of Sciences of the United States of America, 116, 422-427, 10.1073/pnas.1812168116, 2019a.

Li, K., Jacob, D. J., Liao, H., Zhu, J., Shah, V., Shen, L., Bates, K. H., Zhang, Q., and Zhai, S. X.: A two-pollutant strategy for improving ozone and particulate air quality in China, Nature Geoscience, 12, 906-+, 10.1038/s41561-019-0464-x, 2019b.

Li, K., Jacob, D. J., Shen, L., Lu, X., De Smedt, I., and Liao, H.: Increases in surface ozone pollution in China from 2013 to 2019: anthropogenic and meteorological influences, Atmospheric Chemistry and Physics, 20, 11423-11433, 10.5194/acp-20-11423-2020, 2020.

Li, L. Y., Chen, Y., and Xie, S. D.: Spatio-temporal variation of biogenic volatile organic compounds emissions in China, Environmental Pollution, 182, 157-168, 10.1016/j.envpol.2013.06.042, 2013.

Li, M., Zhang, Q., Kurokawa, J., Woo, J. H., He, K. B., Lu, Z. F., Ohara, T., Song, Y., Streets, D. G., Carmichael, G. R., Cheng, Y. F., Hong, C. P., Huo, H., Jiang, X. J., Kang, S. C., Liu, F., Su, H., and Zheng, B.: MIX: a mosaic Asian anthropogenic emission inventory under the international collaboration framework of the MICS-Asia and HTAP, Atmospheric Chemistry and Physics, 17, 935-963, 10.5194/acp-17-935-2017, 2017.

Li, M., Liu, H., Geng, G. N., Hong, C. P., Liu, F., Song, Y., Tong, D., Zheng, B., Cui, H. Y., Man, H. Y., Zhang, Q., and He, K. B.: Anthropogenic emission inventories in China: a review (vol 4, pg 834, 2017), National Science Review, 5, 603-603, 10.1093/nsr/nwy044, 2018a.

Li, S., Wang, T. J., Huang, X., Pu, X., Li, M. M., Chen, P. L., Yang, X. Q., and Wang, M. H.: Impact of East Asian Summer Monsoon on Surface Ozone Pattern in China, Journal of Geophysical Research-Atmospheres, 123, 1401-1411, 10.1002/2017jd027190, 2018b. Liu, H. L., Zhang, M. G., and Han, X.: A review of surface ozone source apportionment in China, Atmospheric and Oceanic Science Letters, 13, 470-484, 10.1080/16742834.2020.1768025, 2020.

Liu, S. C., Trainer, M., Fehsenfeld, F. C., Parrish, D. D., Williams, E. J., Fahey, D. W., Hubler, G., and Murphy, P. C.: Ozone production in the rural troposphere and the implications for regional and global ozone distributions, Journal of Geophysical Research-Atmospheres, 92, 4191-4207, 10.1029/JD092iD04p04191, 1987.

Liu, X. H., Zhang, Y., Xing, J., Zhang, Q. A., Wang, K., Streets, D. G., Jang, C., Wang, W. X., and Hao, J. M.: Understanding of regional air pollution over China using CMAQ, part II. Process analysis and sensitivity of ozone and particulate matter to precursor emissions, Atmospheric Environment, 44, 3719-3727, 10.1016/j.atmosenv.2010.03.036, 2010.

Lu, H. X., Lyu, X. P., Cheng, H. R., Ling, Z. H., and Guo, H.: Overview on the spatial-temporal characteristics of the ozone formation regime in China, Environmental Science-Processes & Impacts, 21, 916-929, 10.1039/c9em00098d, 2019a.

Lu, X., Hong, J. Y., Zhang, L., Cooper, O. R., Schultz, M. G., Xu, X. B., Wang, T., Gao, M., Zhao, Y. H., and Zhang, Y. H.: Severe Surface Ozone Pollution in China: A Global Perspective, Environmental Science & Technology Letters, 5, 487-494, 10.1021/acs.estlett.8b00366, 2018.

Lu, X., Zhang, L., Chen, Y. F., Zhou, M., Zheng, B., Li, K., Liu, Y. M., Lin, J. T., Fu, T. M., and Zhang, Q.: Exploring 2016-2017 surface ozone pollution over China: source contributions and meteorological influences, Atmospheric Chemistry and Physics, 19, 8339-8361, 10.5194/acp-19-8339-2019, 2019b.

Mailler, S., Khvorostyanov, D., and Menut, L.: Impact of the vertical emission profiles on background gas-phase pollution simulated from the EMEP emissions over Europe, Atmospheric Chemistry and Physics, 13, 5987-5998, 10.5194/acp-13-5987-2013, 2013.

Mann, G. W., Carslaw, K. S., Spracklen, D. V., Ridley, D. A., Manktelow, P. T., Chipperfield, M. P., Pickering, S. J., and Johnson, C. E.: Description and evaluation of GLOMAP-mode: a modal global aerosol microphysics model for the UKCA composition-climate model, Geoscientific Model Development, 3, 519-551, 10.5194/gmd-3-519-2010, 2010.

Mertens, M., Kerkweg, A., Grewe, V., Jockel, P., and Sausen, R.: Are contributions of emissions to ozone a matter of scale? - a study using MECO(n) (MESSy v2.50), Geoscientific Model Development, 13, 363-383, 10.5194/gmd-13-363-2020, 2020.

Monks, P. S., Archibald, A. T., Colette, A., Cooper, O., Coyle, M., Derwent, R., Fowler, D., Granier, C., Law, K. S., Mills, G. E., Stevenson, D. S., Tarasova, O., Thouret, V., von Schneidemesser, E., Sommariva, R., Wild, O., and Williams, M. L.: Tropospheric ozone and its precursors from the urban to the global scale from air quality to short-lived climate forcer, Atmospheric Chemistry and Physics, 15, 8889-8973, 10.5194/acp-15-8889-2015, 2015.

Neu, J. L., Prather, M. J., and Penner, J. E.: Global atmospheric chemistry: Integrating over fractional cloud cover, Journal of Geophysical Research-Atmospheres, 112, 10.1029/2006jd008007, 2007.

O'Connor, F. M., Johnson, C. E., Morgenstern, O., Abraham, N. L., Braesicke, P., Dalvi, M., Folberth, G. A., Sanderson, M. G., Telford, P. J., Voulgarakis, A., Young, P. J., Zeng, G., Collins, W. J., and Pyle, J. A.: Evaluation of the new UKCA climate-composition model - Part 2: The Troposphere, Geoscientific Model Development, 7, 41-91, 10.5194/gmd-7-41-2014, 2014.

Pacifico, F., Harrison, S. P., Jones, C. D., Arneth, A., Sitch, S., Weedon, G. P., Barkley, M. P., Palmer, P. I., Serca, D., Potosnak, M., Fu, T. M., Goldstein, A., Bai, J., and Schurgers, G.: Evaluation of a photosynthesis-based biogenic isoprene emission scheme in JULES and simulation of isoprene emissions under present-day climate conditions, Atmospheric Chemistry and Physics, 11, 4371-4389, 10.5194/acp-11-4371-2011, 2011.

Petersen, A. K., Brasseur, G. P., Bouarar, I., Flemming, J., Gauss, M., Jiang, F., Kouznetsov, R., Kranenburg, R., Mijling, B., Peuch, V. H., Pommier, M., Segers, A., Sofiev, M., Timmermans, R., van der A, R., Walters, S., Xie, Y., Xu, J. M., and Zhou, G. Q.: Ensemble forecasts of air quality in eastern China - Part 2: Evaluation of the MarcoPolo-Panda prediction system, version 1, Geoscientific Model Development, 12, 1241-1266, 10.5194/gmd-12-1241-2019, 2019.

Reynolds, R. W., Smith, T. M., Liu, C., Chelton, D. B., Casey, K. S., and Schlax, M. G.: Daily high-resolution-blended analyses for sea surface temperature, Journal of Climate, 20, 5473-5496, 10.1175/2007jcli1824.1, 2007.

470 Sellar, A. A., Jones, C. G., Mulcahy, J. P., Tang, Y. M., Yool, A., Wiltshire, A., O'Connor, F. M., Stringer, M., Hill, R., Palmieri, J., Woodward, S., de Mora, L., Kuhlbrodt, T., Rumbold, S. T., Kelley, D. I., Ellis, R., Johnson, C. E., Walton, J., Abraham, N. L., Andrews, M. B., Andrews, T., Archibald, A. T., Berthou, S., Burke, E., Blockley, E., Carslaw, K., Dalvi, M., Edwards, J., Folberth, G. A., Gedney, N., Griffiths, P. T., Harper, A. B., Hendry, M. A., Hewitt, A. J., Johnson, B., Jones, A., Jones, C. D., Keeble, J., Liddicoat, S., Morgenstern, O., Parker, R. J., Predoi, V., Robertson, E., Siahaan, A., Smith, R. S., Swaminathan, R., Woodhouse, M. T., Zeng, G., and Zerroukat, M.:

475 UKESM1: Description and Evaluation of the UK Earth System Model, Journal of Advances in Modeling Earth Systems, 11, 4513-4558, 10.1029/2019ms001739, 2019.

Sillman, S., Logan, J. A., and Wofsy, S. C.: The sensitivity of ozone to nitrogen-oxides and hydrocarbons in regional ozone episodes, Journal of Geophysical Research-Atmospheres, 95, 1837-1851, 10.1029/JD095iD02p01837, 1990.

Sillman, S.: The use of NOy, H2O2, and HNO3 as indicators for ozone-NOx-hydrocarbon sensitivity in urban locations, Journal of Geo-

480 physical Research-Atmospheres, 100, 14175-14188, 10.1029/94jd02953, 1995.

Sillman, S.: The relation between ozone, NOx and hydrocarbons in urban and polluted rural environments, Atmospheric Environment, 33, 1821-1845, 10.1016/s1352-2310(98)00345-8, 1999.

Sillman, S., and West, J. J.: Reactive nitrogen in Mexico City and its relation to ozone-precursor sensitivity: results from photochemical models, Atmospheric Chemistry and Physics, 9, 3477-3489, 10.5194/acp-9-3477-2009, 2009.

485 Silver, B., Reddington, C. L., Arnold, S. R., and Spracklen, D. V.: Substantial changes in air pollution across China during 2015-2017, Environmental Research Letters, 13, 10.1088/1748-9326/aae718, 2018.

Sindelarova, K., Granier, C., Bouarar, I., Guenther, A., Tilmes, S., Stavrakou, T., Muller, J. F., Kuhn, U., Stefani, P., and Knorr, W.: Global data set of biogenic VOC emissions calculated by the MEGAN model over the last 30 years, Atmospheric Chemistry and Physics, 14, 9317-9341, 10.5194/acp-14-9317-2014, 2014.

490 Stock, Z. S., Russo, M. R., and Pyle, J. A.: Representing ozone extremes in European megacities: the importance of resolution in a global chemistry climate model, Atmospheric Chemistry and Physics, 14, 3899-3912, 10.5194/acp-14-3899-2014, 2014.

Su, R., Lu, K. D., Yu, J. Y., Tan, Z. F., Jiang, M. Q., Li, J., Xie, S. D., Wu, Y. S., Zeng, L. M., Zhai, C. Z., and Zhang, Y. H.: Exploration of the formation mechanism and source attribution of ambient ozone in Chongqing with an observation-based model, Science China-Earth Sciences, 61, 23-32, 10.1007/s11430-017-9104-9, 2018.

495 Tan, Z. F., Lu, K. D., Jiang, M. Q., Su, R., Wang, H. L., Lou, S. R., Fu, Q. Y., Zhai, C. Z., Tan, Q. W., Yue, D. L., Chen, D. H., Wang, Z. S., Xie, S. D., Zeng, L. M., and Zhang, Y. H.: Daytime atmospheric oxidation capacity in four Chinese megacities during the photochemically polluted season: a case study based on box model simulation, Atmospheric Chemistry and Physics, 19, 3493-3513, 10.5194/acp-19-3493-2019, 2019.

Thornton, J. A., Wooldridge, P. J., Cohen, R. C., Martinez, M., Harder, H., Brune, W. H., Williams, E. J., Roberts, J. M., Fehsenfeld, F. C.,

500 Hall, S. R., Shetter, R. E., Wert, B. P., and Fried, A.: Ozone production rates as a function of NOx abundances and HOx production rates in the Nashville urban plume, Journal of Geophysical Research-Atmospheres, 107, 10.1029/2001jd000932, 2002.

Valari, M., and Menut, L.: Does an Increase in Air Quality Models' Resolution Bring Surface Ozone Concentrations Closer to Reality?, Journal of Atmospheric and Oceanic Technology, 25, 1955-1968, 10.1175/2008jtecha1123.1, 2008.

van der Werf, G. R., Randerson, J. T., Giglio, L., Collatz, G. J., Mu, M., Kasibhatla, P. S., Morton, D. C., DeFries, R. S., Jin, Y., and van

505 Leeuwen, T. T.: Global fire emissions and the contribution of deforestation, savanna, forest, agricultural, and peat fires (1997-2009), Atmospheric Chemistry and Physics, 10, 11707-11735, 10.5194/acp-10-11707-2010, 2010.

von Schneidemesser, E., Monks, P. S., Allan, J. D., Bruhwiler, L., Forster, P., Fowler, D., Lauer, A., Morgan, W. T., Paasonen, P., Righi, M., Sindelarova, K., and Sutton, M. A.: Chemistry and the Linkages between Air Quality and Climate Change, Chemical Reviews, 115, 3856-3897, 10.1021/acs.chemrev.5b00089, 2015.

510 Walters, D., Baran, A. J., Boutle, I., Brooks, M., Earnshaw, P., Edwards, J., Furtado, K., Hi, P., Lock, A., Manners, J., Morcrette, C., Mulcahy, J., Sanchez, C., Smith, C., Stratton, R., Tennant, W., Tomassini, L., Van Weverberg, K., Vosper, S., Willett, M., Browse, J., Bushell, A., Carslaw, K., Dalvi, M., Essery, R., Gedney, N., Hardiman, S., Johnson, B., Johnson, C., Jones, A., Jones, C., Mann, G., Milton, S., Rumbold, H., Sellar, A., Ujiie, M., Whitall, M., Williams, K., and Zerroukat, M.: The Met Office Unified Model Global Atmosphere 7.0/7.1 and JULES Global Land 7.0 configurations, Geoscientific Model Development, 12, 1909-1963, 10.5194/gmd-12-1909-2019, 2019.

515 Wang, J. H., Ge, B. Z., and Wang, Z. F.: Ozone Production Efficiency in Highly Polluted Environments, Current Pollution Reports, 4, 198-207, 10.1007/s40726-018-0093-9, 2018.

Wang, N., Lyu, X. P., Deng, X. J., Huang, X., Jiang, F., and Ding, A. J.: Aggravating O3 pollution due to NOx emission control in eastern China, Science of the Total Environment, 677, 732-744, 10.1016/j.scitotenv.2019.04.388, 2019.

Wang, T., Xue, L. K., Brimblecombe, P., Lam, Y. F., Li, L., and Zhang, L.: Ozone pollution in China: A review of concentrations, meteoro-
520 logical influences, chemical precursors, and effects, Science of the Total Environment, 575, 1582-1596, 10.1016/j.scitotenv.2016.10.081, 2017.

Wild, O., and Prather, M. J.: Global tropospheric ozone modeling: Quantifying errors due to grid resolution, Journal of Geophysical Research-Atmospheres, 111, 10.1029/2005jd006605, 2006.

Wu, R. R., and Xie, S. D.: Spatial Distribution of Ozone Formation in China Derived from Emissions of Speciated Volatile Organic Com-
525 pounds, Environmental Science & Technology, 51, 2574-2583, 10.1021/acs.est.6b03634, 2017.

Xing, J., Ding, D., Wang, S. X., Dong, Z. X., Kelly, J. T., Jang, C., Zhu, Y., and Hao, J. M.: Development and application of observable response indicators for design of an effective ozone and fine-particle pollution control strategy in China, Atmospheric Chemistry and Physics, 19, 13627-13646, 10.5194/acp-19-13627-2019, 2019.

Young, P. J., Naik, V., Fiore, A. M., Gaudel, A., Guo, J., Lin, M. Y., Neu, J. L., Parrish, D. D., Rieder, H. E., Schnell, J. L., Tilmes, S., Wild,
530 O., Zhang, L., Ziemke, J., Brandt, J., Delcloo, A., Doherty, R. M., Geels, C., Hegglin, M. I., Hu, L., Im, U., Kumar, R., Luhar, A., Murray, L., Plummer, D., Rodriguez, J., Saiz-Lopez, A., Schultz, M. G., Woodhouse, M. T., and Zeng, G.: Tropospheric Ozone Assessment Report: Assessment of global-scale model performance for global and regional ozone distributions, variability, and trends, Elementa-Science of the Anthropocene, 6, 10.1525/elementa.265, 2018.

Zhao, C., Wang, Y. H., Yang, Q., Fu, R., Cunnold, D., and Choi, Y.: Impact of East Asian summer monsoon on the air quality over China:
535 View from space, Journal of Geophysical Research-Atmospheres, 115, 10.1029/2009jd012745, 2010.

Zhao, Y. H., Zhang, L., Zhou, M., Chen, D., Lu, X., Tao, W., Liu, J. F., Tian, H., Ma, Y. P., and Fu, T. M.: Influences of planetary boundary layer mixing parameterization on summertime surface ozone concentration and dry deposition over North China, Atmospheric Environment, 218, 10.1016/j.atmosenv.2019.116950, 2019.

Zheng, B., Tong, D., Li, M., Liu, F., Hong, C. P., Geng, G. N., Li, H. Y., Li, X., Peng, L. Q., Qi, J., Yan, L., Zhang, Y. X., Zhao, H. Y.,
540 Zheng, Y. X., He, K. B., and Zhang, Q.: Trends in China's anthropogenic emissions since 2010 as the consequence of clean air actions, Atmospheric Chemistry and Physics, 18, 14095-14111, 10.5194/acp-18-14095-2018, 2018.